

Article

The Investigation of Triple-Lithiated Transition Metal Oxides Synthesized from the Spent LiCoO₂

Alexandra Kosenko ^{*}, Konstantin Pushnitsa, Vladislav Chernyavsky, Pavel Novikov and Anatoliy A. Popovich

Institute of Machinery, Materials and Transport, Peter the Great Saint-Petersburg Polytechnic University, 195221 Saint Petersburg, Russia

^{*} Correspondence: kosenko_aa@spbstu.ru

Abstract: The environmentally friendly closed cycle of the regeneration process of spent LiCoO₂ was successfully developed and the following synthesis of triple-lithiated transition metal oxides was carried out. A hydrometallurgy recycling route with the usage of 1.5 mol/L of malic acid and 3 vol.% of H₂O₂ as a leaching solution for cobalt extraction was chosen. The efficiency of the cobalt extraction reached 95%. The obtained material was investigated using an X-ray diffraction analysis and the EDX and SEM methods. The electrochemical behavior of the synthesized NCM111 was analyzed and compared to the commercially available material of the same type. The material demonstrated a specific discharge capacity on the first cycle of 163.7 mAh/g. The cyclic resource of the material turned out to be unsatisfactory. In addition, perspective cathode materials, such as NCM622 and NCM811, were obtained. The synthesized materials were analyzed using XRD, SEM, EDX, charge-discharge and cycle life tests, and the CVA and EIS methods. The initial specific discharge capacities of the NCM622 and NCM811 were 168 and 187 mAh/g, respectively. On the fifth cycle, the NCM622 demonstrated an increasing capacity—to 179 mAh/g, unlike NCM811, as the capacity of this material decreased to 141 mAh/g.



Citation: Kosenko, A.; Pushnitsa, K.; Chernyavsky, V.; Novikov, P.; Popovich, A.A. The Investigation of Triple-Lithiated Transition Metal Oxides Synthesized from the Spent LiCoO₂. *Batteries* **2023**, *9*, 423. <https://doi.org/10.3390/batteries9080423>

Academic Editors: Chiara Ferrara and Elza Bontempi

Received: 17 July 2023

Revised: 3 August 2023

Accepted: 10 August 2023

Published: 12 August 2023



Copyright: © 2023 by the authors. Licensee MDPI, Basel, Switzerland. This article is an open access article distributed under the terms and conditions of the Creative Commons Attribution (CC BY) license (<https://creativecommons.org/licenses/by/4.0/>).

Keywords: cobalt extraction; LiCoO₂; triple-lithiated transition metal oxides; regeneration; spent lithium-ion batteries

1. Introduction

The use of lithium-ion batteries has increased significantly in recent years, as, due to their high-energy density, they have found applications in many areas, such as electronic devices, energy storage systems, and electric vehicles. After a thousand charge–discharge cycles, their cycle life comes to an end [1], they become unsuitable for the correct operation of portable devices, and they are then subject to disposal/burial [2]. If battery waste is not treated properly, it poses a serious environmental hazard, due to the toxic chemicals such as heavy metals (Co, Ni, and Cu, etc.) contained in the cathode/anode, and organic solvents and fluorinated compounds contained in the electrolyte [3–5]. In fact, researchers have realized the importance of recycling and seen commercial opportunities in this area. The recycling of spent LIB has attracted a lot of attention in both academic and industrial fields, and the technologies developed over the past years are rapidly transforming [6]. In addition, when using LIBs in large quantities with high growth rates of the use of this technology, a significant depletion of the raw materials and limited natural resources of metals (for example, Co) threaten the sustainable manufacturing of batteries [7]. The recycling of used batteries can reduce the load from both ecological pollution and the lack of resources in the long term. Due to the limited resources of the materials used in the cell and the environmental problems after the termination of the use of LIB, the post-processing of the valuable metals from spent batteries is essential.

As the most valuable metals are concentrated in the cathode materials, the focus of recycling spent LIBs is the recovery of the metals from the waste cathode materials.

Conventionally, industrial technologies for the regeneration of cathode materials from spent batteries consist of three steps [8]:

- Cathode materials and aluminum current collectors division using the dissolution method, heat treatment method, dissolution in an alkaline solution method, mechanical method, or separation by ultrasound;
- The separation and extraction of the target metals (e.g., Co, Ni, Mn, Cu, Fe, and Li) from the cathode mass [9];
- The synthesis of new cathode material.

However, the established technologies in the industrial sector for processing cathode active materials from battery waste have significant disadvantages [10,11]:

- There are many complex separation stages and, in general, the processing paths are often complicated;
- Some valuable materials may be lost in the recycling process;
- Secondary pollution takes place due to the impurities' removal and metal ion precipitation by using various solvents, such as acids and alkalis in most recycling processes;
- The high consumption of chemicals during processing, low extraction efficiency of the valuable metal elements from the end-of-life cathode materials, expensive solvents, and complex processing methods hinder the large-scale application of hydrometallurgical technology in industry;
- In the process of pyrometallurgical processing (i.e., melting), only cobalt, iron, copper, and nickel are extracted in the form of alloys or molten metals, and the main components such as lithium are not extracted, which are lost in the form of slag. Moreover, the recovered alloys require further hydrometallurgical purification;
- At the end of the hydrometallurgical recycling process, wastewater is discharged, which must be disposed of.

As is mentioned above, in the description of the established technologies, three main routes [12,13] for LIB recycling exist: pyrometallurgy [14,15], hydrometallurgy [16,17], and biometallurgy [18]. For this study, the hydrometallurgy strategy was chosen, which allows for the closed-loop recycling process and final products of a high purity to be obtained. The hydrometallurgical route includes leaching (acid or alkali), purification and separation steps, and product recovery. The comparison table of the already studied usages of inorganic and organic acids for the leaching process is presented in Table 1.

Table 1. Comparison of different acid-leaching methods.

Leaching Solution	Initial Material	Resulting Material	Ref.
DL-malic acid + H ₂ O ₂	LCO	LCO	[19]
Phosphoric acid; citric acid; acetic acid 4 mol/L H ₂ SO ₄ + H ₂ O ₂	NCM523; CMB LCO	Li ⁺ , Ni ²⁺ , Co ²⁺ , Mn ²⁺ Co(OH) ₂ ; Li ₂ SO ₄	[20] [21]
4 mol/L H ₂ SO ₄ + 30 wt% H ₂ O ₂	Mixed cathode materials	Li ₂ CO ₃	[22]
2 mol/L formic acid + 2 vol.% H ₂ O ₂	NCM111	Li ₂ CO ₃	[23]
1 mol/L oxalic acid	NCM523	Li ₂ CO ₃	[24]
2.75 mol/L H ₃ PO ₄	LiNixMnyCo _{1-x-y} O	Li ₃ PO ₄	[25]
0.5 mol/L HCl	LCO	Li ₂ CO ₃ , [CoCl ₄] ²⁻	[26]
2.5 mol/L malic acid by electrolysis	LCO	LCO	[27]
H ₂ SO ₄ + H ₂ O ₂	Mixed cathode materials	NCM	[28]
0.5 mol/L citric acid + 1.5 vol.% H ₂ O ₂	Mixed cathode materials	NCM111	[29]
1.5 mol/L lactic acid + 0.5% H ₂ O ₂	NCM111	NCM111	[30]
Acetic acid, malic acid HNO ₃	Spent LIB LCO	NCM111 Li ⁺ Co ²⁺ , Co ³⁺	[31] [32]
Ascorbic acid	LCO	Li ⁺ Co ²⁺ , Co ³⁺	[33]
Succinic acid + H ₂ O ₂	LCO	Li ⁺ Co ²⁺ , Co ³⁺	[34]
Trichloroacetic acid + H ₂ O ₂	Cathode scraps	NCM111	[35]
Imminodiacetic acid	LCO	Li ⁺ Co ²⁺	[36]

Based on the conducted studies with usage of organic acid, it can be concluded that a new cathode material with good electrochemical features can be successfully recovered

using the sol-gel method [17,29–31,37], in which organic acid can act as both a chelating agent and leaching agent.

Nevertheless, none of the existing studies on the regeneration of cathode materials from spent batteries has considered the strategy of the «closed cycle», in which valuable metal components are regenerated from spent batteries with a LiCoO₂ cathode, and on the basis of the extracted materials, the synthesis of the triple-lithium oxides of cathode materials ($\text{Li}(\text{Ni}_x\text{Co}_y\text{Mn}_z)\text{O}_2$) is carried out.

This work aims at the methodological development of cobalt extraction from spent Li-ion batteries using a hydrometallurgical process with an organic acid leaching solution, which allows for the use of a cobalt-containing leachate with additional salts of Li, Ni, and Mn as a precursor for the following synthesis of triple-lithiated transition metals oxide NCM.

2. Materials and Methods

2.1. Cobalt Extraction and NCM Synthesis

As the initial material, a cathode with an aluminum current collector from a spent lithium-ion battery was used as the cobalt source. The spent battery was fully discharged into a 5% NaCl solution for 24 h, then disassembled, and the cathode was separated from the other parts of the battery. The cathode plates were plunged into an acetone solution for 24 h, washed with distilled water to remove the electrolyte salts, and then dried in a vacuum at 95 °C.

The cathode material was leached in a 1.5 mol/L malic acid solution with 3 vol.% of H₂O₂ at 90 °C with stirring for 1 h. The reaction involved in the leaching was as follows:



The undissolved residue was removed via filtering in order to obtain the leachate solution containing Co²⁺ ions. After this, Ni, Mn, and Li acetates were added to the leachate solution in a stoichiometric ratio in order to subsequently obtain the NCM material. The calculation was carried out in the following way: after the end of the leaching process, the filtrated residue was dried for 24 h and weighted. The obtained mass was subtracted from the initial cathode mass—this was the theoretical dissolved cathode mass in the solution. This value was multiplied by 0.92 to obtain the active mass in the solution. The most common ratio of cathode material: binder PVDF: conductive additive is 92:5:3, which is used while coating on a current collector. Afterwards, the active mass was multiplied by 0.59—this was theoretical cobalt mass in the solution. Then, this value was divided by the Co molar mass (59 g/mol) to obtain the amount of Co²⁺ ions. Furthermore, to calculate the NCM111 amount, the cobalt amount was multiplied by 3. Then, the masses of $\text{Ni}(\text{CH}_3\text{COO})_2 \cdot 4\text{H}_2\text{O}$ (NiAc), $\text{Mn}(\text{CH}_3\text{COO})_2 \cdot 4\text{H}_2\text{O}$ (MnAc), and $\text{CH}_3\text{COOLi} \cdot 2\text{H}_2\text{O}$ (LiAc) were calculated based on the substance amounts (the NiAc and MnAc amounts were equal to the Co amount, and the LiAc value was equal to the NCM111 amount) and respective molar masses. The next step was water evaporation from the resulting solution with the forced removal of gases. The obtained precipitate was used as the precursor for the following synthesis of the NCM cathode material through heat treatment. The scheme of the process is presented on Figure 1. The heat treatment stages are described in more detail in the Supplementary Materials.

2.2. Investigation of the Cobalt Extraction Degree Dependence on the Leaching Time

To analyze the effect of the leaching time on the degree of the cobalt extraction from spent cathode material, 5 samples were taken every 20 min during the leaching and then synthesis was carried out according to the method described in the Section 2.1. Nickel acetate in the amount of 0.5 g was added to the precursors as a comparative element for the following elemental analysis. The graph is presented in the Supplementary Materials.

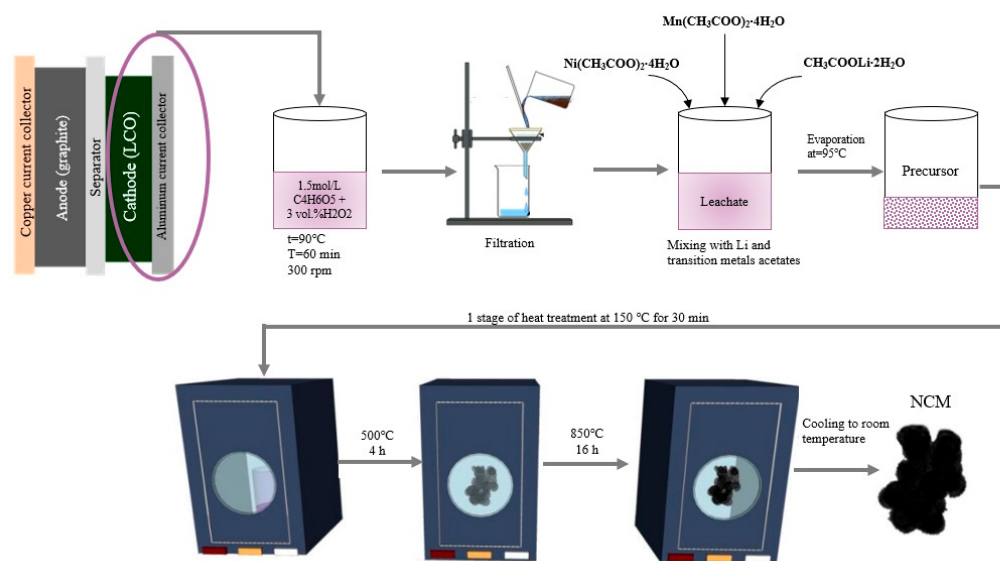


Figure 1. The scheme of leaching process and following synthesis of the new cathode material.

To determine the amount of extracted cobalt, the elemental composition was analyzed using the EDX method.

2.3. Elemental Analysis and Material Characterization

The morphology and microstructure of the synthesized sample were studied using a Mira 3 Tescan scanning electron microscope in the SE (secondary electrons) mode. The chemical composition of the powder was studied on an electron microscope using X-ray spectroscopy with an energy dispersion detector from EDX Oxford Instruments X-Max 80. An X-ray phase analysis of the obtained samples was performed on a Bruker D8 Advance diffractometer ($CuK\alpha = 1.5406 \text{ \AA}$) in the angle range of 15–85 degrees, with a step of 0.030 and an exposure of 0.8 s at each step. The identification of the phase composition was carried out using the DIFFRAC.EVA V5.0 program. The structural parameters were refined using the Rietveld method using TOPAS5 software. The granulometric composition of the sample was analyzed using Fritsch Analysette 22 NanoTec equipment.

To determine the electrochemical behavior of the materials, electrodes were prepared. The composition of the electrode slurry was: 92% of the cathode active material, 3% of PVDF as a binder (trade mark Solef 5130), and 5% of carbon black (SuperP). N-methylpyrrolidone was used as a solvent. The obtained suspension was applied to aluminum foil using the film coater MSK-AFA-III, MTI Corp. The clearance height was 200 μm . The next step was drying the electrodes, followed by rolling for compaction. After that, circles with a diameter of 14 mm were cut out of the electrode sheet to assemble coin cells of the CR2032 type. Lithium metal was used as the anode material, TC-E918 (Tinki), which is a solution of LiPF₆ in a mixture of organic carbonates, was used as an electrolyte, and Celgard 2325 was used as a separator.

The electrochemical characteristics during charging and discharging were measured using the Netware coin cell—5 V 10 mA Battery Test System. The Cyclic voltammetry (CV) and electrochemical impedance spectroscopy (EIS) measurements were carried out on a Cortest CS310 potentiostat. The CV conditions were: scanning speed—0.1 mVs^{-1} ; potential range—2.5–4.3 V; and EIS frequency range—0.01 Hz to 100 kHz.

3. Results

3.1. Characterization of Initial Material

Figure 2 shows a diffractogram of the initial cathode material of the LCO type. Lithium cobalt oxide peaks belonging to the spatial group R3 m are clearly observed. In addition, Co_3O_4 peaks belonging to the Fd-3m group are observed, which can be explained by the

fact that, during the charging process, the $\text{Li}_2\text{O}/\text{Co}$ mixture could be oxidized into Co, and then the $\text{Li}_2\text{O}/\text{CoO}$ mixture could result in the formation of Co_3O_4 in the higher-voltage region [38].

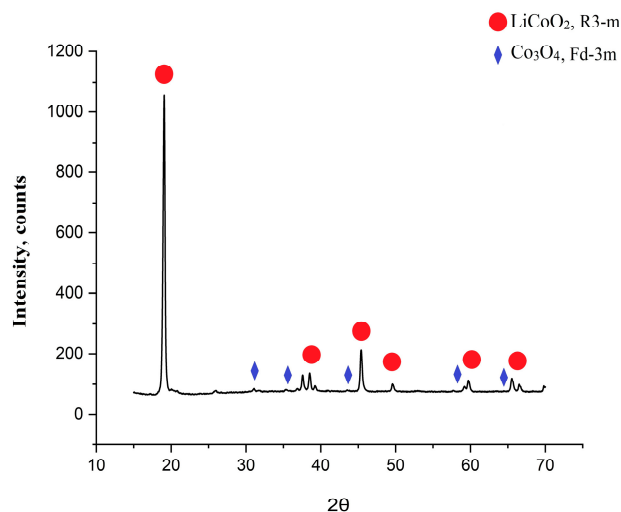


Figure 2. The diffractogram of the initial material.

Table 2 shows the chemical composition in atomic percentages of the starting material obtained using the EDX method.

Table 2. Chemical composition of the initial material in at.%.

	C	O	F	Al	P	S	Ti	Fe	Co	Total
At.%	33.67	34.76	14.61	5.72	1.72	0.12	0.05	1.14	8.21	100.00

Apparently, 8.21 atomic percent of cobalt was present in the material, which made it possible to use this cathode material as a cobalt source for the subsequent extraction. The SEM image of initial material is presented in the Supplementary Materials.

3.2. Analysis of Synthesized Material

Figure 3 shows an X-ray diffractogram of the synthesized cathode material of the NCM111 obtained based on the extracted cobalt, and for comparison, a diffractogram of commercial NCM111 material is also added. The patterns of the synthesized NCM material were indexed to layered oxide with an R-3m space group without any peaks of the impurity phase. The peaks were consistent with the standard card of $\text{Li}(\text{Ni}_{1/3}\text{Co}_{1/3}\text{Mn}_{1/3})\text{O}_2$ (PDF#01-075-9200). The distinct peak split corresponding to the (006)/(102) planes suggests a well-ordered, layered structure.

Additionally, it is highly recommended for cathode materials to be analyzed according to the following parameters [39–41]:

1. The split of the peaks I_{006}/I_{102} ($2\theta \sim 36^\circ$)—this parameter indicates a good ordering of the hexagonal lattice, and peak separation was present both in the synthesized and commercial NCM111.
2. R-factor, $R = (I_{006} + I_{102})/I_{101}$ —the lower the value of this parameter, the higher the ordering of the structure (for good materials < 0.5); for both materials, this parameter was higher than it should have been: for commercial, it was 0.597, and for synthesized, it was 0.866.
3. The ratio I_{003}/I_{104} ($2\theta 003 \sim 20^\circ$, $2\theta 104 \sim 45^\circ$). The smaller this ratio, the closer the lattice is to cubic. In the context of these materials, this parameter characterizes cationic mixing and, for good materials, should be > 1.2 . For the commercial material, it was a little bit higher than that for the obtained (1543 and 1442, respectively).

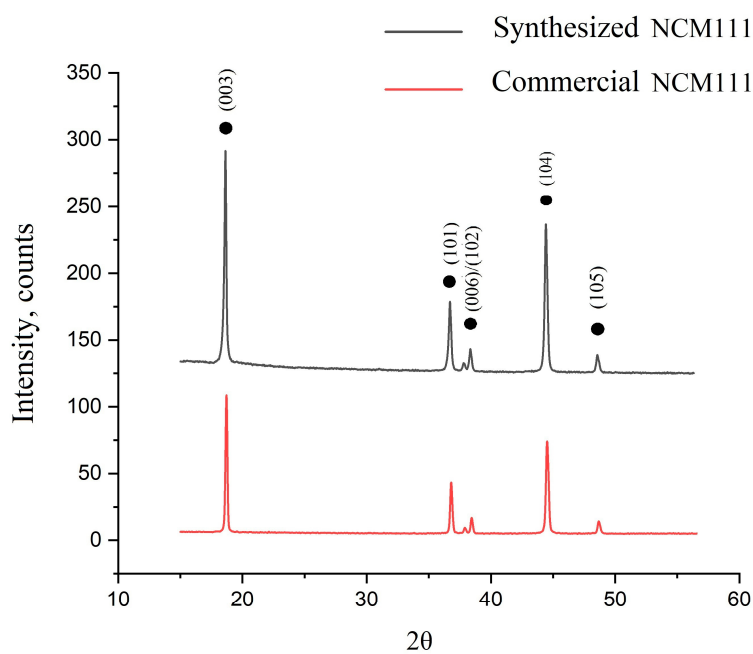


Figure 3. The diffractogram of the synthesized material and the comparative diffractogram of the commercial NCM111.

Obviously, the R-factor of the obtained NCM materials after the cobalt extraction was extremely high for these types of materials. Probably, this could have been a result of the influence of the sol-gel synthesis on the powder structure. The ratio of the 003 and 104 peaks was lower than the ratio of the commercial material, but still more than 1.2; hence, the crystal lattice was hexagonal. The structural parameters of both materials are presented in the Supplementary Materials.

Figure 4 demonstrates the results of the morphology study of the synthesized sample obtained using scanning electron microscopy in the secondary electron mode. Apparently, the powder had rounded particles with an average particle size of 300 nm^{-1} microns, with a uniform particle size distribution. In addition, the agglomeration of particles in the sample was quite high. It is well known that a small particle size and uniform size distribution contribute to the rapid migration of Li^+ ions, which can contribute to obtaining excellent electrochemical characteristics [42].

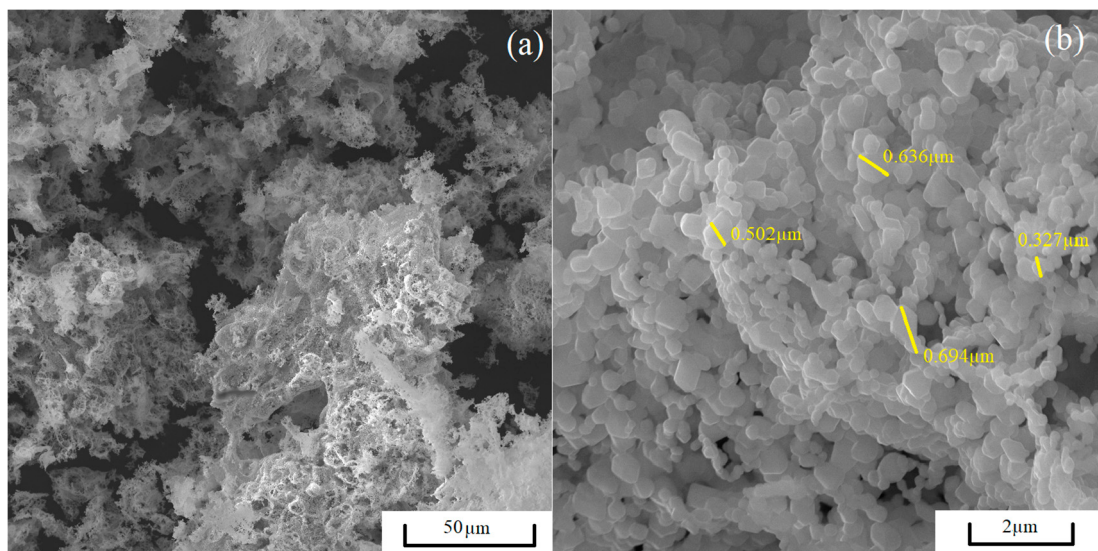


Figure 4. The SEM photographs of the obtained material. (a)— $\times 1000$, and (b)— $\times 20,000$.

In Table 3, the particle size distribution is presented. The material was prepared before the analysis of the particle size distribution via grinding in an agate mortar.

Table 3. Particle size distribution of synthesized material.

	D10	D50	D90
Average particle size, μm	1.3	5.7	14.7

The chemical composition of the obtained material was analyzed using energy dispersive X-ray spectroscopy. The results are presented in Table 4.

Table 4. Results of EDX analysis of synthesized NCM.

Element	Ni	Co	Mn	O	C	Al	Total
At.%	10.91	9.41	10.91	61.56	6.79	0.744	100

Thus, the atomic ratio of the transition metals in the synthesized material was $\text{Li}(\text{Ni}_{0.35}\text{Co}_{0.3}\text{Mn}_{0.35})\text{O}_2$, which is quite close to the theoretically calculated NCM111. In the synthesized material, the amount of cobalt was slightly less than that theoretically calculated, which resulted in a shift in the atomic ratio towards the added nickel and manganese. The cobalt in the composition of layered cathode materials of the NCM type is responsible for increasing their kinetics, low-temperature properties, initial discharge capacity, and thermal stability [43]. A low cobalt content is likely to degrade these characteristics.

3.3. Electrochemical Characteristics of Obtained Material

The electrochemical characteristics of the obtained material are illustrated in Figure 5. Figure 5a shows the charge/discharge curves at the 1st and 10th cycles at a current rate of 0.1 C and in the voltage range of 2.8–4.3 V for the synthesized (SNCM) and 2.6–4.3 V for the commercial (CNCM) materials. The synthesized material at the 1st cycle demonstrated a charging capacity of 164.7 mAh/g, a discharge capacity of 163.7 mAh/g, and the Coulomb efficiency for the 1st cycle was 99%, while the capacities for the 10th cycle were 158.2 and 159.4, respectively. The Coulomb efficiency of the material being close to 100% at all 10 cycles indicated a reversible intercalation/deintercalation of the lithium. A slight drop in the capacity during the cycling indicated a sufficient stability of the structure. The shape of the charge–discharge curves was typical for layered cathode materials and there was no clearly defined discharge area. The commercial material at the 1st cycle demonstrated a charging capacity of 153.0 mAh/g, a discharge capacity of 133.0 mAh/g, and the Coulomb efficiency for the 1st cycle was 87%, while for the 10th cycle, the capacities were 140.9 and 139.6, respectively, and the Coulomb efficiency was 99%. Hence, the synthesized NCM111 was not inferior in terms of its electrochemical characteristics compared to the commercially available material of such a type.

The cyclic resource of the material was also investigated and the results are illustrated in Figure 5b. At the 1st cycle, the charge and discharge capacities were 137.73 and 136.16 mAh/g, and at the 60th cycle, the charging and discharging capacities were 112.21 and 107.0 mAh/g, respectively. The capacity loss over 60 cycles was 21.5%. This drop in capacity during the cycling can be explained by the sufficiently high value of the R-factor (0.866), since this parameter indicates that the structure in the sample was not ordered.

In addition, for the obtained material, a current load study was carried out with subsequent relaxation to determine the stability of the material structure, and the results are demonstrated in Figure 5c. The material was tested with discharge currents corresponding to five-hour, one-hour, and twenty-minute discharges. The discharge was carried out with a current of 0.2 C for the first eight cycles. The drop in capacity relative to the five-hour discharge cycle, for discharge with a current of 1 C, was 61%, and with a current of 3 C, it was 43%. When discharged with a current of 0.2 C after 24 cycles of current load,

the material was close to the initial capacity values, which meant that the material was quite stable.

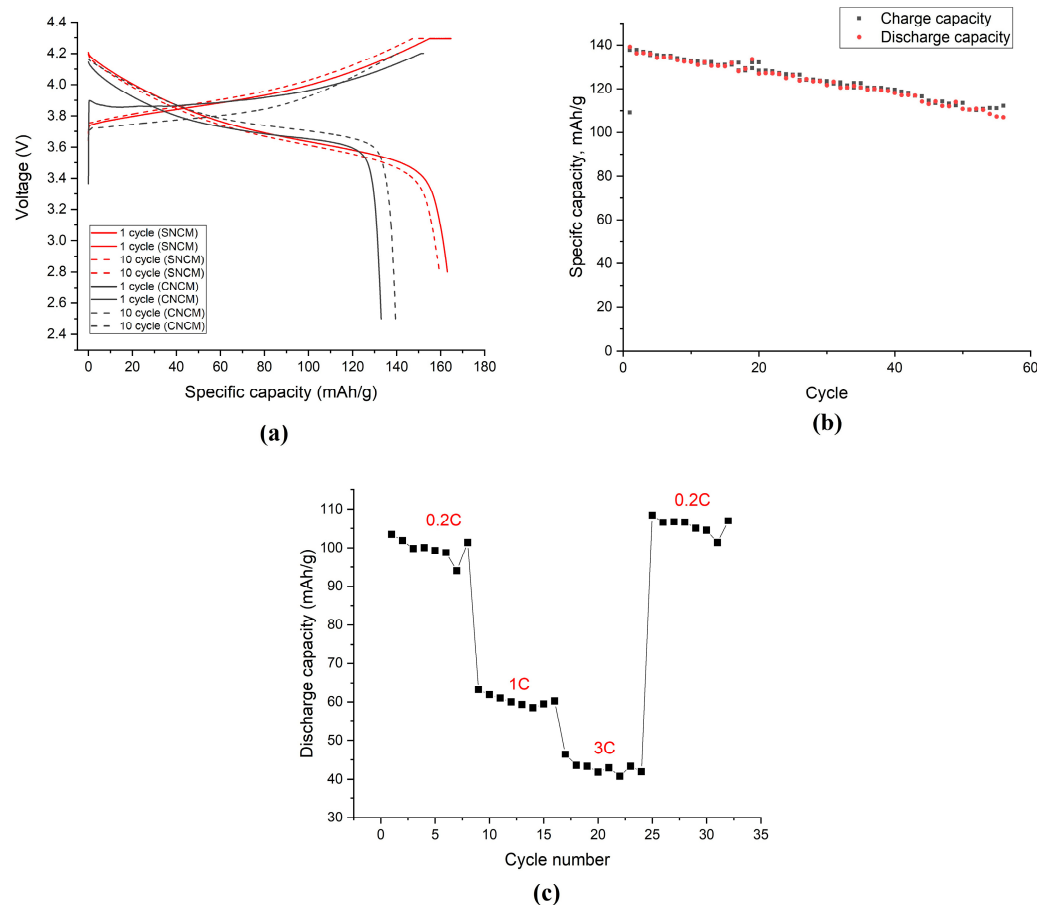


Figure 5. The electrochemical analysis of the obtained NCM111: (a)—charge–discharge curves at 1st and 10th cycles, (b)—cyclic test, and (c)—different current load study.

3.4. Comparison of 2 NCM Materials of Different Chemistry Type, Synthesized Using Developed Methodology

To analyze the possibility of using the developed methodology for the cobalt extraction in a consequent synthesis of perspective NCM material, two comparative iterations were carried out: syntheses of NCM622 and NCM811. The chemical and phase compositions, morphology, structure, and electrochemical characteristics of the obtained materials were investigated.

The synthesis method was the same as that described in Section 2.1, except with regard to NCM811. The heat treatment of this precursor was carried out in a tube furnace in oxygen flow, with a flow rate of 20 mL/min. The necessity of heat treatment in oxygen ambience is explained by the fact that, with a lack of oxygen (in air atmosphere), nonstoichiometric oxide lithium–nickel is formed ($\text{Li}_{(1-z)}\text{Ni}_{(1+z)}\text{O}_2$) [44]. If this phase is present in synthesized material, at the 1st cycle of charge–discharge, the additional Ni^{2+} ions ($1 + z$) will cause structure destruction, which leads to poor electrochemical behavior of the material. The effect of nonstoichiometric lithium–nickel oxide forming was investigated, and it was found that Ni^{2+} is formed in a lack of oxygen, instead of Ni^{3+} , and the Ni^{2+} is stable. Based on this fact, to decrease the forming of such undesired oxides, the synthesis of Ni-rich cathode materials should be carried out in oxygen flow.

The synthesized NCM622 and NCM811 cathodes' powders were analyzed in terms of particle size distribution and the results are presented in Table 5. The materials were prepared before the analysis of the particle size distribution via grinding in an agate mortar. In total, 90% of the particles were less than 35.3 mkm for NCM622 and less

than 29.1 mkm for the NCM811 material. These values were greater than those of the commercial materials, but the following treatment, such as milling and granulation, will probably increase the characteristics.

Table 5. The particle size distribution of obtained materials.

	NCM622	NCM811
D10, μm	6.6	1.9
D50, μm	18.3	12.1
D90, μm	35.3	29.1

A comparative diffractogram of the synthesized materials is presented in Figure 6. Obviously, typical peaks of the phase of triple-lithiated transition metal oxide NCM are observed in the two synthesized materials. All the materials had a separation of peaks 006/102 and 108/110, which indicates a good ordering of the layered structure of the materials. Due to the heat treatment of the precursor for the synthesis of the NCM811 material in oxygen flow, it was possible to obtain a material with a good crystallinity.

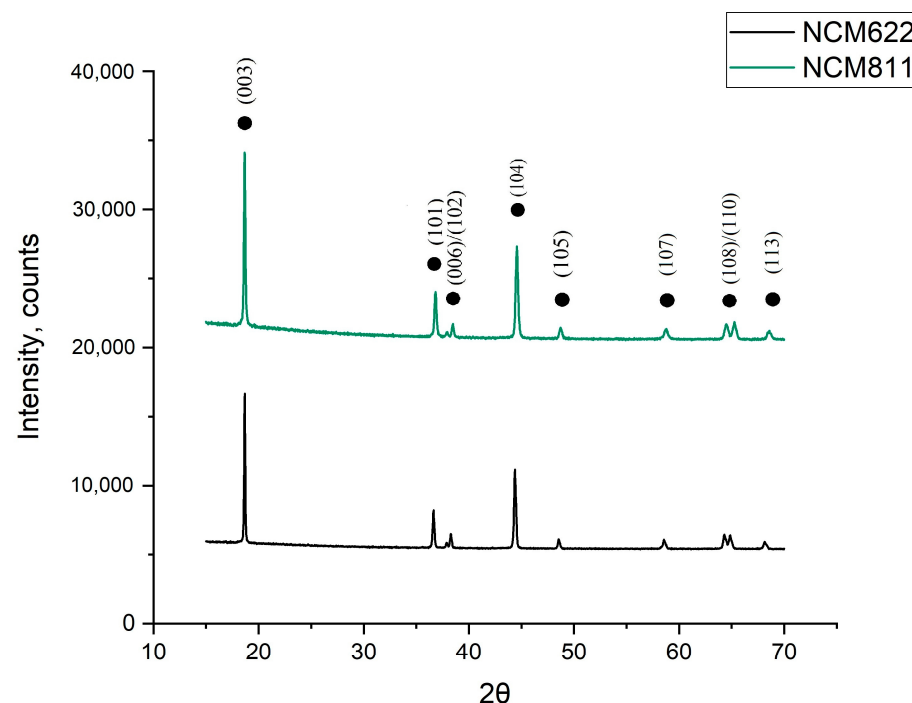


Figure 6. The comparative diffractogram of the synthesized materials.

The values of the R-factor for all the materials turned out to be lower than that of the material described in Section 3.3; for NCM622, it was 0.739, and for NCM811, it was 0.685. At the same time, the ratio of peaks 003/104 in the NCM811 material was significantly lower than that in the other cathode material, at 1.896 vs. 1.372. This phenomenon is explained by the fact that the amount of nickel relative to the amount of lithium in 811 was greater than that in the other cathode materials, as a result of which, the cationic mixing of nickel and lithium ions was more expressed, the layered structure was less ordered, and it could be assumed that the capacitance characteristics of this material would be worse. The structural parameters of both materials are presented in the Supplementary Materials.

The scanning electron microphotographs of the obtained NCM622 and NCM811 materials in the secondary electron mode are illustrated in Figure 7. Figure 7a,b illustrate NCM622. It is apparent that the material consisted of rounded particles with a size of 0.5–1 microns, and also that the particles were agglomerated. The NCM811 microphotographs are presented in Figure 7c,d. The particles of this material were fragmented, and

this fact can be explained by the bigger amount of nickel in its composition. At a high magnification, it can be observed that the sintered fragmented particles consisted of small particles of the same f shape, with sizes ranging from 0.5 to 1 microns.

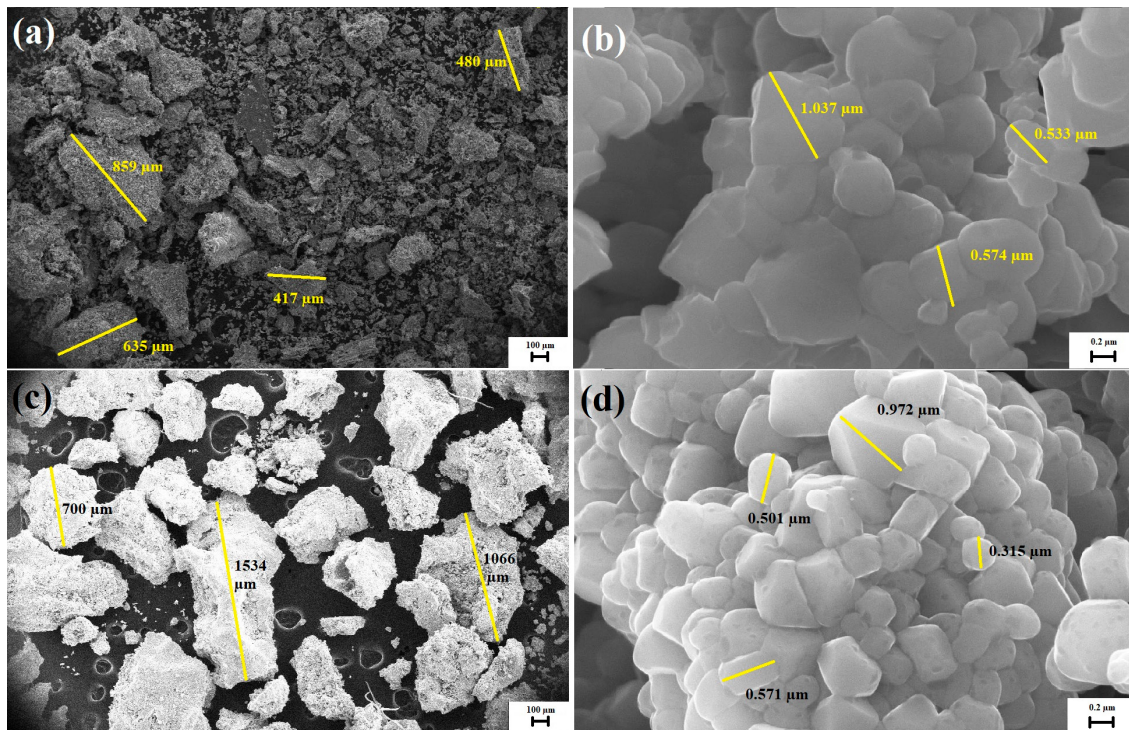


Figure 7. The SEM photographs of the obtained materials. (a,b)—NCM622, (c,d)—NCM811.

The chemical composition of the synthesized materials in terms of atomic percentage is presented in Table 6.

Table 6. Chemical composition of the synthesized materials in at.%.

Sample	Ni	Co	Mn	Al	Total
NCM622	60.00	17.27	21.47	1.26	100
NCM811	79.51	9.55	9.62	1.33	100

Thus, the atomic ratio of the transition metals in the obtained materials for the calculated NCM622 was $\text{LiNi}_{0.60}\text{Co}_{0.17}\text{Mn}_{0.22}\text{O}_2$, and for the calculated NCM811, was $\text{LiNi}_{0.80}\text{Co}_{0.10}\text{Mn}_{0.10}\text{O}_2$. The obtained results were close to the theoretically calculated ratios, and there was a slightly reduced cobalt content relative to that theoretically calculated, which was likely to affect the initial capacitance characteristics. There was also the presence of more than 1% aluminum, which probably got into the precursor during the extraction of the cobalt from the aluminum current collector. The introduction of an Al^{3+} ion increased the Ni^{3+} ratio and limited the mixing of cations. Compared to the unmodified samples, the cathode material NCM811 doped with Al^{3+} demonstrated an excellent cycling performance with a capacity retention of 70% at 10 °C after 1000 charge–discharge cycles [45]. In addition, doping in the precursor was useful for reducing the energy potential, which led to a more uniform distribution of elements and a reduction in binding deficiencies during the subsequent calcination process. It is noteworthy that the alloying of Al could suppress the effect of cationic mixing and reduce the destruction of the structure of the material during charging [46].

3.5. Electrochemical Behavior of NCM622 and NCM811

Figure 8 illustrates the electrochemical behavior of the synthesized NCM622 and NCM811. In Figure 8a, charge–discharge curves at a current rate of 0.1 C and in a voltage range of 2.8–4.3 V at the 1st and 5th cycles are presented. The initial charging and discharge capacities of the NCM622 were 169 and 168 mAh/g, and those of the NCM811 were 235 and 187 mAh/g, respectively. The Coulomb efficiency for 622 was 99%, and for 811, was 80%. At cycle 5, the charging and discharging capacities for NCM622 were 180 and 179, and for NCM811, were 146 and 141 mAh/g, respectively. The Coulomb efficiency for NCM622 was 99.3%, and for NCM811, it was 96.5%. The unsatisfactory capacitance characteristics of material 811 after five cycles were explained by the low ordering of the structure and the high cationic mixing. The increase in capacity on cycle 5 for material 622 may have been because of working out the active mass.

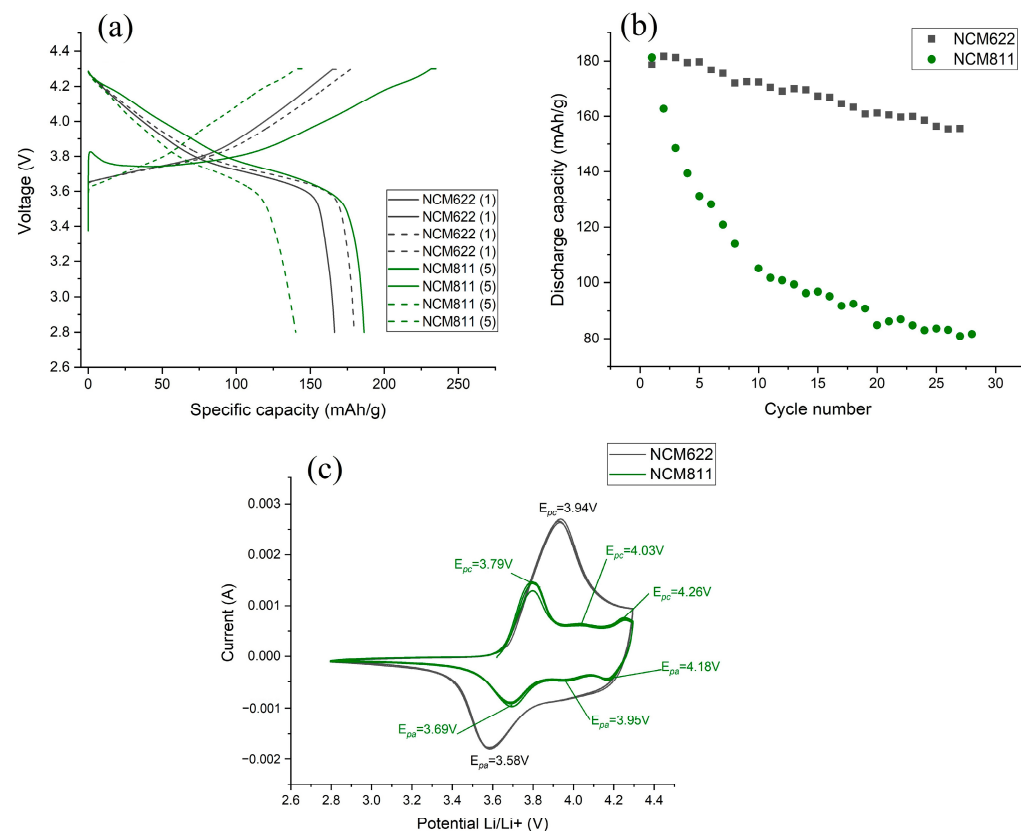


Figure 8. Electrochemical analysis of the synthesized cathode materials. (a)—charge–discharge curves at 1st and 5th cycles, (b)—the cycling test, and (c)—CVA polarization curves.

The Coulomb efficiency of the material being close to 100% indicates a reversible intercalation/deintercalation of the lithium, indicating a sufficient stability of the structure. The shape of the charge–discharge curves was typical for layered cathode materials and there was no clearly defined discharge area. The medium-discharge voltage of the material NCM622 was higher than that of NCM811, which indicates that the material had higher energy intensity values. At the same time, the charging curve of 622 was lower than that of 811, which indicates a low internal resistance of the material.

Both synthesized materials were analyzed for a cyclic resource and the resulting graph is presented in Figure 8b. The capacity drop in NCM622 for 28 cycles was 13% and in NCM811 it was 55%. The large drop in the capacity of the NCM811 was due to the high cationic mixing, which had an extremely negative effect on the capacitance characteristics of the material.

The synthesized materials were also investigated using cyclic voltammetry and the polarization curves are shown in Figure 8c. This method for analyzing the electrochemical

characteristics of a material allows for the reversibility of the electrode reactions to be analyzed, whether side reactions are present on the electrode to be determined, and also allows for the kinetics of the electrode reactions in different materials to be compared. The peak of the cathode potential was 3.94 V, and that of the anode potential was 3.58 V. According to the literature [47], those peaks refer to a reversible intercalation of the Li^+ ions. In the cathode and anode regions for the NCM622 material, the peaks of the potentials of the reversible process of the deintercalation/intercalation of the lithium ions are clearly observed. The peak of the cathode potential was 3.94 V and that of the anode potential was 3.58 V. Peaks of side electrode reactions were not observed.

Peaks of reversible intercalation/deintercalation potentials were also observed for the material NCM811. The cathode peak was present at 3.79 V, and the anode peak at 3.69 V. In addition to these, there were also less obvious redox peaks at 4.03/3.95 V and 4.26/4.18 V, which appeared during the charge due to multiphase transitions from hexagonal to monoclinic (H1/M), from monoclinic to hexagonal (M/H2), and from hexagonal to hexagonal (H2/H3) [48]. The absence of an H2/H3 phase transition with a lower Ni content in the material NCM622 indicated a good reversibility of the electrode and significantly affected the stability of the material structure, which also explained the lower loss of capacitance during charge/discharge of the material NCM622.

3.6. Electrochemical Impedance Spectroscopy Investigation

The impedance of the cathode materials obtained was investigated in a two-electrode cell, which was a CR2032 tablet layout, where lithium foil was used as an antielectrode. The impedance measurement was carried out on the Correct CS310 installation in the frequency range from 1.5×10^5 Hz to 0.01 Hz. The measurements were carried out in the infected state up to a potential of 4.3 V and the amplitude of the oscillations was 10 mV. The modeling of the impedance spectra was carried out using the ZView program. The impedance hodographs of the studied samples are presented in Figure 9. It is worth noting that usually when modeling impedance, an equivalent circuit is used, as shown in Figure 10. In this diagram, R1 is the resistance of the cell elements: the housing, spacers, and other components, R2 is the resistance of the CEI film (cathode electrolyte interface), and R3 is the charge transfer resistance. Each block of elements is characterized by a semicircle on the impedance hodograph.

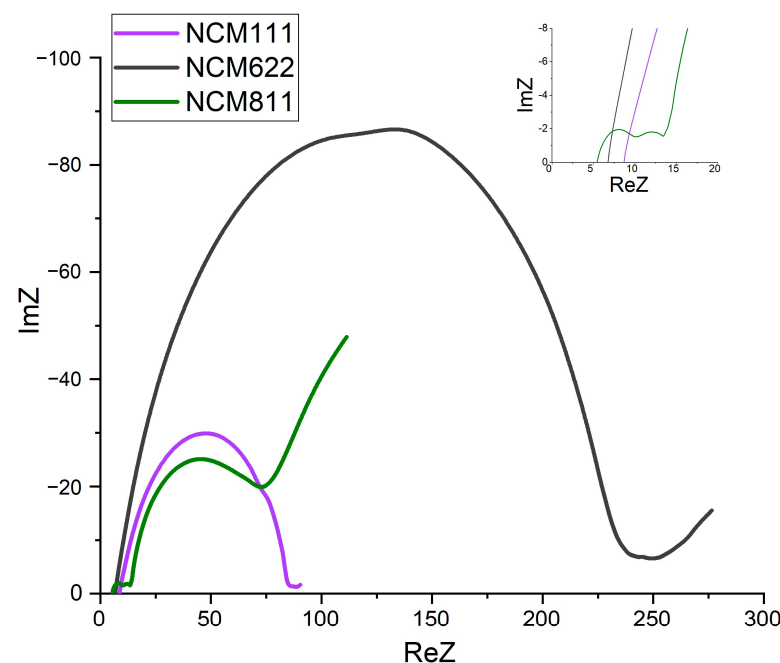


Figure 9. The hodographs of the impedance of the studied samples.

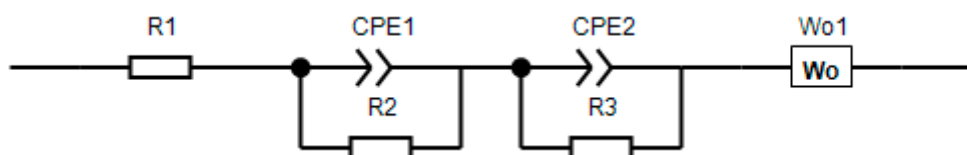


Figure 10. The equivalent scheme used at the impedance modeling.

It is worth noting that, for samples NCM 111 and 622, there was no semicircle in the high-frequency region of the spectrum associated with the CEI response. For NCM 811, three semicircles can be observed, instead of two classic ones. Taking into account the corresponding forms of impedance hodographs, the simulation was carried out according to the schemes shown in Figure 11. It can be assumed that a different shape of the hodograph for NCM 811 is associated with phase transitions, which were also noticeable on the CVA graphs. Since the equivalent circuits were used differently, it is proposed to compare the total resistance of the samples, minus R1, since it did not relate to the material under study (Table 7).

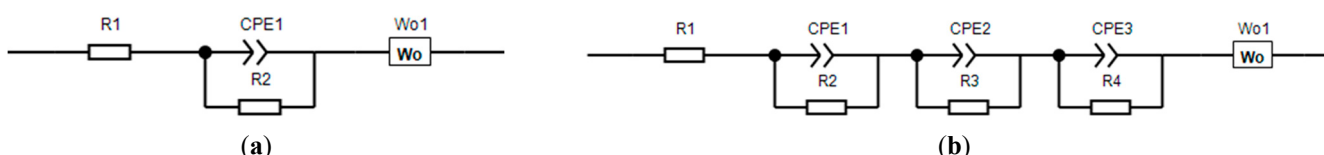


Figure 11. The equivalent schemes: (a)—for samples NCM111 and NCM622; (b)—for NCM811.

Table 7. Total resistance of the samples.

	NCM111	NCM622	NCM811
R _{sum} , Ohm	74.368	223.91	38.6474

From the presented data, the sample NCM622 had the highest total resistance. The other two samples were comparable, but the sample NCM811 had the least resistance. In addition, since the “tail” of diffusion was the largest in this sample, this also indicates better kinetics for this material. Sample modeling parameters are presented in the Supplementary Materials.

4. Conclusions

This paper described the synthesis of different types of triple-lithiated transition metal oxides from spent LiCoO₂, with use of extracted cobalt malate and Ni, Mn, and Li acetates using the sol-gel method, followed by a three-stage thermal treatment. The obtained material was investigated using different methods, such as XRD, SEM, and EDX. The initial capacities of the synthesized NCM111 were equal to 163.7 mAh/g and 159.4 mAh/g at the 10th cycle, under a current rate of 0.1 C. The resulting values corresponded to the requirements of commercial materials of the same type. The cycle life study of the material showed a drop of 21.5% after 60 cycles, which could be explained by the high value of the R-factor and disorder of the layered structure. The different current load study demonstrated that the obtained NCM111 was stable.

To analyze the possibility of using the developed synthesis method for obtaining perspective cathode materials, such as NCM622 and NCM811, two comparative iterations were carried out. The synthesis of NCM811 was carried out in oxygen flow to minimize the formation of nonstoichiometric oxide Li_(1-z)Ni_(1+z)O₂, which could lead to structure destruction and as a result, poor electrochemical behavior of the material. The obtained materials were investigated using different analytical methods, such as XRD, SEM, EDX, CVA, and EIS. The initial discharge capacities of NCM622 and NCM811 were 169 and 187 mAh/g, respectively. The drop of capacity in the cycling tests was 13% for NCM 622 and 55% for 811 after 28 cycles. Such a big drop in the NCM811 capacity could be explained by the layered structure disorder and high cation mixing in the material. On the

polarization curves of the NCM622m symmetric peaks of a reversible redox reaction were observed in the area of 3.6–3.8 V. There were no signs of adverse reactions. For NCM811, besides the peaks of the redox reactions in the area of 3.6–3.7 V, there were also two peaks around 4 and 4.2 V, which could be attributed to a series of phase transitions in the material, which took place during the charge–discharge process, leading to local destruction in the crystal lattice and, as a result, to the fast capacity drop during the cycling.

The developed strategy allowed the shortening of the regeneration process of spent cathode materials. In addition, it became possible to obtain a dissimilar material compared to the initial one. The results of our research represented that the electrochemical behavior of the regenerated materials was comparable to that of the commercial ones.

Organic acids can be used for the extraction of a wide range of metals. Thus, the suggested approach of the usage an organic acids solution both for the extraction and the subsequent synthesis via the sol-gel method can be applicable for obtaining materials of various classes.

Supplementary Materials: The following supporting information can be downloaded at: <https://www.mdpi.com/article/10.3390/batteries9080423/s1>; Figure S1: The diagram of the heat treatment stages; Figure S2: The SEM image of initial LCO material; Figure S3: The dependence of the extracted mass of cobalt on the leaching time; Table S1: Averaged results of elemental analysis of 5 samples of synthesized material in at.%; Table S2: Structural parameters of crystal lattices for commercial and synthesized material; Table S3: Structural parameters of crystal lattices for NCM622 and NCM811; Table S4: Sample modeling parameters.

Author Contributions: Conceptualization, A.K. and K.P.; methodology, A.K. and K.P.; formal analysis, A.K.; investigation, A.K., K.P. and V.C.; resources, A.A.P.; data curation, A.K. and K.P.; writing—original draft preparation, A.K.; writing—review and editing, V.C.; visualization, A.K.; supervision, P.N.; project administration, P.N. and A.A.P.; funding acquisition, A.A.P. All authors have read and agreed to the published version of the manuscript.

Funding: The research was funded by the Ministry of Science and Higher Education of the Russian Federation by «Agreement on the grant in the form of subsidies from the federal budget for the implementation of state support for the creation and development of world-class scientific centers, those are performing research and development on the priorities of scientific and technological development» dated 20 April 2022 No. 075-15-2022-311.

Data Availability Statement: The data presented in this study are available upon request from the corresponding author. The data are not publicly available due to corporate confidentiality requirements.

Conflicts of Interest: The authors declare no conflict of interest.

References

1. Jin, S.; Liang, J.; Mu, D.; Lin, T.; Tian, Y.; Zhang, J.; Wang, Y.; Chen, M.; Shi, Q.; Dai, C. Structural Evolution of Layered Oxide Cathodes for Spent Li-Ion Batteries: Degradation Mechanism and Repair Strategy. *SusMat* **2023**, *3*, 362–378. [[CrossRef](#)]
2. Han, X.; Lu, L.; Zheng, Y.; Feng, X.; Li, Z.; Li, J.; Ouyang, M. A Review on the Key Issues of the Lithium Ion Battery Degradation among the Whole Life Cycle. *eTransportation* **2019**, *1*, 100005. [[CrossRef](#)]
3. Yu, J.; He, Y.; Li, H.; Xie, W.; Zhang, T. Effect of the Secondary Product of Semi-Solid Phase Fenton on the Flotability of Electrode Material from Spent Lithium-Ion Battery. *Powder Technol.* **2017**, *315*, 139–146. [[CrossRef](#)]
4. Assefi, M.; Maroufi, S.; Yamauchi, Y.; Sahajwalla, V. Pyrometallurgical Recycling of Li-Ion, Ni–Cd and Ni–MH Batteries: A Minireview. *Curr. Opin. Green Sustain. Chem.* **2020**, *24*, 26–31. [[CrossRef](#)]
5. Qu, X.; Cai, M.; Zhang, B.; Xie, H.; Guo, L.; Wang, D.; Yin, H. A Vapor Thermal Approach to Selective Recycling of Spent Lithium-Ion Batteries. *Green Chem.* **2021**, *23*, 8673–8684. [[CrossRef](#)]
6. Fan, M.; Chang, X.; Meng, Q.; Wan, L.; Guo, Y. Progress in the Sustainable Recycling of Spent Lithium-ion Batteries. *SusMat* **2021**, *1*, 241–254. [[CrossRef](#)]
7. Zeng, X.; Li, J. On the Sustainability of Cobalt Utilization in China. *Resour. Conserv. Recycl.* **2015**, *104*, 12–18. [[CrossRef](#)]
8. Yu, W.; Guo, Y.; Shang, Z.; Zhang, Y.; Xu, S. A Review on Comprehensive Recycling of Spent Power Lithium-Ion Battery in China. *eTransportation* **2022**, *11*, 100155. [[CrossRef](#)]
9. Natarajan, S.; Aravindan, V. Recycling Strategies for Spent Li-Ion Battery Mixed Cathodes. *ACS Energy Lett.* **2018**, *3*, 2101–2103. [[CrossRef](#)]

10. Kim, S.; Bang, J.; Yoo, J.; Shin, Y.; Bae, J.; Jeong, J.; Kim, K.; Dong, P.; Kwon, K. A Comprehensive Review on the Pretreatment Process in Lithium-Ion Battery Recycling. *J. Clean. Prod.* **2021**, *294*, 126329. [[CrossRef](#)]
11. Jin, S.; Mu, D.; Lu, Z.; Li, R.; Liu, Z.; Wang, Y.; Tian, S.; Dai, C. A Comprehensive Review on the Recycling of Spent Lithium-Ion Batteries: Urgent Status and Technology Advances. *J. Clean. Prod.* **2022**, *340*, 130535. [[CrossRef](#)]
12. Bae, H.; Kim, Y. Technologies of Lithium Recycling from Waste Lithium Ion Batteries: A Review. *Mater. Adv.* **2021**, *2*, 3234–3250. [[CrossRef](#)]
13. Wagner-Wenz, R.; van Zuilichem, A.-J.; Göllner-Völker, L.; Berberich, K.; Weidenkaff, A.; Schebek, L. Recycling Routes of Lithium-Ion Batteries: A Critical Review of the Development Status, the Process Performance, and Life-Cycle Environmental Impacts. *MRS Energy Sustain.* **2022**, *10*, 1–34. [[CrossRef](#)]
14. Yang, H.; Deng, B.; Jing, X.; Li, W.; Wang, D. Direct Recovery of Degraded LiCoO₂ Cathode Material from Spent Lithium-Ion Batteries: Efficient Impurity Removal toward Practical Applications. *Waste Manag.* **2021**, *129*, 85–94. [[CrossRef](#)]
15. Tao, R.; Xing, P.; Li, H.; Sun, Z.; Wu, Y. Recovery of Spent LiCoO₂ Lithium-Ion Battery via Environmentally Friendly Pyrolysis and Hydrometallurgical Leaching. *Resour. Conserv. Recycl.* **2022**, *176*, 105921. [[CrossRef](#)]
16. Yu, J.; Ma, B.; Shao, S.; Wang, C.; Chen, Y.; Zhang, W. Cobalt Recovery and Microspherical Cobalt Tetroxide Preparation from Ammonia Leaching Solution of Spent Lithium-Ion Batteries. *Trans. Nonferrous Met. Soc. China* **2022**, *32*, 3136–3148. [[CrossRef](#)]
17. Yao, L.; Feng, Y.; Xi, G. A New Method for the Synthesis of LiNi_{1/3}Co_{1/3}Mn_{1/3}O₂ from Waste Lithium Ion Batteries. *RSC Adv.* **2015**, *5*, 44107–44114. [[CrossRef](#)]
18. Bahaloo-Horeh, N.; Vakilchian, F.; Mousavi, S.M. Bio-Hydrometallurgical Methods For Recycling Spent Lithium-Ion Batteries. In *Recycling of Spent Lithium-Ion Batteries*; Springer International Publishing: Cham, Switzerland, 2019; pp. 161–197.
19. Zhou, S.; Zhang, Y.; Meng, Q.; Dong, P.; Fei, Z.; Li, Q. Recycling of LiCoO₂ Cathode Material from Spent Lithium Ion Batteries by Ultrasonic Enhanced Leaching and One-Step Regeneration. *J. Environ. Manag.* **2021**, *277*, 111426. [[CrossRef](#)]
20. Song, D.; Wang, T.; Liu, Z.; Zhao, S.; Quan, J.; Li, G.; Zhu, H.; Huang, J.; He, W. Characteristic Comparison of Leaching Valuable Metals from Spent Power Li-Ion Batteries for Vehicles Using the Inorganic and Organic Acid System. *J. Environ. Chem. Eng.* **2022**, *10*, 107102. [[CrossRef](#)]
21. Aktas, S.; Fray, D.J.; Burheim, O.; Fenstad, J.; Açıma, E. Recovery of Metallic Values from Spent Li Ion Secondary Batteries. *Miner. Process. Extr. Metall.* **2006**, *115*, 95–100. [[CrossRef](#)]
22. Zou, H.; Gratz, E.; Apelian, D.; Wang, Y. A Novel Method to Recycle Mixed Cathode Materials for Lithium Ion Batteries. *Green Chem.* **2013**, *15*, 1183. [[CrossRef](#)]
23. Gao, W.; Zhang, X.; Zheng, X.; Lin, X.; Cao, H.; Zhang, Y.; Sun, Z. Lithium Carbonate Recovery from Cathode Scrap of Spent Lithium-Ion Battery: A Closed-Loop Process. *Environ. Sci. Technol.* **2017**, *51*, 1662–1669. [[CrossRef](#)] [[PubMed](#)]
24. Li, Q.; Fung, K.Y.; Xu, L.; Wibowo, C.; Ng, K.M. Process Synthesis: Selective Recovery of Lithium from Lithium-Ion Battery Cathode Materials. *Ind. Eng. Chem. Res.* **2019**, *58*, 3118–3130. [[CrossRef](#)]
25. Xiao, J.; Li, J.; Xu, Z. Challenges to Future Development of Spent Lithium Ion Batteries Recovery from Environmental and Technological Perspectives. *Environ. Sci. Technol.* **2020**, *54*, 9–25. [[CrossRef](#)] [[PubMed](#)]
26. Xu, L.; Chen, C.; Fu, M.-L. Separation of Cobalt and Lithium from Spent Lithium-Ion Battery Leach Liquors by Ionic Liquid Extraction Using Cyphos IL-101. *Hydrometallurgy* **2020**, *197*, 105439. [[CrossRef](#)]
27. Zhou, S.; Zhang, Y.; Meng, Q.; Dong, P.; Yang, X.; Liu, P.; Li, Q.; Fei, Z. Recycling of Spent LiCoO₂ Materials by Electrolytic Leaching of Cathode Electrode Plate. *J. Environ. Chem. Eng.* **2021**, *9*, 104789. [[CrossRef](#)]
28. Zheng, R.; Wang, W.; Dai, Y.; Ma, Q.; Liu, Y.; Mu, D.; Li, R.; Ren, J.; Dai, C. A Closed-Loop Process for Recycling LiNi_xCo_yMn_(1-x-y)O₂ from Mixed Cathode Materials of Lithium-Ion Batteries. *Green Energy Environ.* **2017**, *2*, 42–50. [[CrossRef](#)]
29. Li, L.; Bian, Y.; Zhang, X.; Guan, Y.; Fan, E.; Wu, F.; Chen, R. Process for Recycling Mixed-Cathode Materials from Spent Lithium-Ion Batteries and Kinetics of Leaching. *Waste Manag.* **2018**, *71*, 362–371. [[CrossRef](#)]
30. Li, L.; Fan, E.; Guan, Y.; Zhang, X.; Xue, Q.; Wei, L.; Wu, F.; Chen, R. Sustainable Recovery of Cathode Materials from Spent Lithium-Ion Batteries Using Lactic Acid Leaching System. *ACS Sustain. Chem. Eng.* **2017**, *5*, 5224–5233. [[CrossRef](#)]
31. Li, L.; Bian, Y.; Zhang, X.; Xue, Q.; Fan, E.; Wu, F.; Chen, R. Economical Recycling Process for Spent Lithium-Ion Batteries and Macro- and Micro-Scale Mechanistic Study. *J. Power Sources* **2018**, *377*, 70–79. [[CrossRef](#)]
32. Lee, C.K.; Rhee, K.-I. Reductive Leaching of Cathodic Active Materials from Lithium Ion Battery Wastes. *Hydrometallurgy* **2003**, *68*, 5–10. [[CrossRef](#)]
33. Li, L.; Lu, J.; Ren, Y.; Zhang, X.X.; Chen, R.J.; Wu, F.; Amine, K. Ascorbic-Acid-Assisted Recovery of Cobalt and Lithium from Spent Li-Ion Batteries. *J. Power Sources* **2012**, *218*, 21–27. [[CrossRef](#)]
34. Li, L.; Qu, W.; Zhang, X.; Lu, J.; Chen, R.; Wu, F.; Amine, K. Succinic Acid-Based Leaching System: A Sustainable Process for Recovery of Valuable Metals from Spent Li-Ion Batteries. *J. Power Sources* **2015**, *282*, 544–551. [[CrossRef](#)]
35. Zhang, X.; Cao, H.; Xie, Y.; Ning, P.; An, H.; You, H.; Nawaz, F. A Closed-Loop Process for Recycling LiNi_{1/3}Co_{1/3}Mn_{1/3}O₂ from the Cathode Scraps of Lithium-Ion Batteries: Process Optimization and Kinetics Analysis. *Sep. Purif. Technol.* **2015**, *150*, 186–195. [[CrossRef](#)]
36. Nayaka, G.P.; Pai, K.V.; Manjanna, J.; Keny, S.J. Use of Mild Organic Acid Reagents to Recover the Co and Li from Spent Li-Ion Batteries. *Waste Manag.* **2016**, *51*, 234–238. [[CrossRef](#)] [[PubMed](#)]
37. Yao, L.; Yao, H.; Xi, G.; Feng, Y. Recycling and Synthesis of LiNi_{1/3}Co_{1/3}Mn_{1/3}O₂ from Waste Lithium Ion Batteries Using d, l-Malic Acid. *RSC Adv.* **2016**, *6*, 17947–17954. [[CrossRef](#)]

38. Shu, J.; Shui, M.; Huang, F.; Ren, Y.; Wang, Q.; Xu, D.; Hou, L. A New Look at Lithium Cobalt Oxide in a Broad Voltage Range for Lithium-Ion Batteries. *J. Phys. Chem. C* **2010**, *114*, 3323–3328. [[CrossRef](#)]
39. Zybert, M.; Ronduda, H.; Dąbrowska, K.; Ostrowski, A.; Sobczak, K.; Moszyński, D.; Hamankiewicz, B.; Rogulski, Z.; Raróg-Pilecka, W.; Wieczorek, W. Suppressing Ni/Li Disordering in $\text{LiNi}_{0.6}\text{Mn}_{0.2}\text{Co}_{0.2}\text{O}_2$ Cathode Material for Li-Ion Batteries by Rare Earth Element Doping. *Energy Rep.* **2022**, *8*, 3995–4005. [[CrossRef](#)]
40. Reimers, J.N.; Li, W.; Dahn, J.R. Short-Range Cation Ordering in $\text{Li}_x\text{Ni}_{2-x}\text{O}_2$. *Phys. Rev. B* **1993**, *47*, 8486–8493. [[CrossRef](#)]
41. Skvortsova, I.; Savina, A.A.; Orlova, E.D.; Gorshkov, V.S.; Abakumov, A.M. Microwave-Assisted Hydrothermal Synthesis of Space Fillers to Enhance Volumetric Energy Density of NMC811 Cathode Material for Li-Ion Batteries. *Batteries* **2022**, *8*, 67. [[CrossRef](#)]
42. Zhang, J.; Qiao, J.; Sun, K.; Wang, Z. Balancing Particle Properties for Practical Lithium-Ion Batteries. *Particuology* **2022**, *61*, 18–29. [[CrossRef](#)]
43. Chu, R.; Zou, Y.; Zhu, P.; Tan, S.; Qiu, F.; Fu, W.; Niu, F.; Huang, W. Progress of Single-Crystal Nickel-Cobalt-Manganese Cathode Research. *Energies* **2022**, *15*, 9235. [[CrossRef](#)]
44. Delmas, C.; Pérès, J.P.; Rougier, A.; Demourgues, A.; Weill, F.; Chadwick, A.; Broussely, M.; Perton, F.; Biensan, P.; Willmann, P. On the Behavior of the Li_xNiO_2 System: An Electrochemical and Structural Overview. *J. Power Sources* **1997**, *68*, 120–125. [[CrossRef](#)]
45. Li, Y.-C.; Xiang, W.; Wu, Z.-G.; Xu, C.-L.; Xu, Y.-D.; Xiao, Y.; Yang, Z.-G.; Wu, C.-J.; Lv, G.-P.; Guo, X.-D. Construction of Homogeneously Al^{3+} Doped Ni Rich Ni-Co-Mn Cathode with High Stable Cycling Performance and Storage Stability via Scalable Continuous Precipitation. *Electrochim. Acta* **2018**, *291*, 84–94. [[CrossRef](#)]
46. Cheng, L.; Zhang, B.; Su, S.-L.; Ming, L.; Zhao, Y.; Tan, X.-X. Al-Doping Enables High Stability of Single-Crystalline $\text{LiNi}_{0.7}\text{Co}_{0.1}\text{Mn}_{0.2}\text{O}_2$ Lithium-Ion Cathodes at High Voltage. *RSC Adv.* **2021**, *11*, 124–128. [[CrossRef](#)]
47. Gu, S.; He, T.; Kong, J.; Fu, T.; Guo, Z.; Cui, J.; Chen, Z. Regeneration of NCM622 from End-of-Life Lithium-Ion Battery Cathode Materials. *RSC Adv.* **2023**, *13*, 906–913. [[CrossRef](#)]
48. Woo, S.-U.; Yoon, C.S.; Amine, K.; Belharouak, I.; Sun, Y.-K. Significant Improvement of Electrochemical Performance of AlF_3 -Coated $\text{LiNi}_{0.8}\text{Co}_{0.1}\text{Mn}_{0.1}\text{O}_2$ Cathode Materials. *J. Electrochem. Soc.* **2007**, *154*, A1005. [[CrossRef](#)]

Disclaimer/Publisher’s Note: The statements, opinions and data contained in all publications are solely those of the individual author(s) and contributor(s) and not of MDPI and/or the editor(s). MDPI and/or the editor(s) disclaim responsibility for any injury to people or property resulting from any ideas, methods, instructions or products referred to in the content.